Achieving high strength and high ductility in nanostructured metals: Experiment and modelling

Linli Zhu,[1,2,a)] Aiying Chen,[3] and Jian Lu[4,b)]

[1)] *Institute of Applied Mechanics, School of Aeronautics and Astronautics, Zhejiang University, 310007, Hangzhou, Zhejiang Province, China*

[2)] *Department of Mechanical Engineering, The Hong Kong Polytechnic University, Kowloon, Hong Kong, China*

[3)] *School of Material Science and Engineering, Shanghai Institute of Technology, 201400, Shanghai, China*

[4)] *Department of Mechanical and Biomedical Engineering, City University of Hong Kong, Kowloon, Hong Kong, China*

(Received 17 February 2012; accepted 22 February 2012; published online 10 March 2012)

Abstract Engineering nanostructures in metallic materials such as nanograins and nanotwins can promote plastic performance significantly. Nano/ultrafine-grained metals embedded in coarse grains called bimodal metals and nanotwinned polycrystalline metals have been proved to possess extensively improved yield strength whilst keeping good ductility. This paper will present an experimental study on nanostructured stainless steel prepared by surface mechanical attrition treatment (SMAT) with surface impacts of lower strain rate ($10\ s^{-1}$–$10^3\ s^{-1}$) and higher strain rate ($10^4\ s^{-1}$–$10^5\ s^{-1}$). Microstructure transition has been observed from the original γ-austenite coarse grains to α'-martensite nanograins with bimodal grain size distribution for lower strain rates to nanotwins in the ultrafine/coarse grained austenite phase for higher strain rates. Meanwhile, we will further address the mechanism-based plastic models to describe the yield strength, strain hardening and ductility in nanostructured metals with bimodal grain size distribution and nanotwinned polycrystalline metals. The proposed theoretical models can comprehensively describe the plastic deformation in these two kinds of nanostructured metals and excellent agreement is achieved between the numerical and experimental results. These models can be utilized to optimize the strength and ductility in nanostructured metals by controlling the size and distribution of nanostructures. © *2012 The Chinese Society of Theoretical and Applied Mechanics.* [doi:10.1063/2.1202101]

Keywords nanostructured metal, bimodal grain size distribution, nanotwinned metal, yield strength, ductility, strain hardening

I. INTRODUCTION

The combination of high strength and moderate ductility has been emerging as an essential challenge in the application of metals and alloys in modern technologies.[1] Materials possessing higher strength can be prepared by several widely used strategies such as the refinement of grain size, solid solution alloying and plastic straining, but most of the existing strengthening technologies often lead to low tensile ductility.[2,3] With the development of nanoscience and nanotechnology, there are two kinds of methodologies appearing to efficiently achieve high strength and good ductility at the same time in metallic materials by involving nanostructures such as nanograins and nanotwins. The first methodology is to embed the coarse grains into the nanograined matrix phase to construct nanostructured metals/alloys with bimodal grain size distribution.[4] In these materials, the high strength comes from the nanograined matrix phase, and the coarse grains provide the tensile elongation by preventing the propagation of the nano/microcracks that arise in the nanograined phase. The second is to engineer coherent internal boundaries such as the twin boundaries at the nanometre scale in polycrystalline metals.[2,5,6] By decreasing the twin spacing to the nanometre scale, the yield strength and ductility are both improved in these kinds of metals. In the past ten years, nanotwinned metals and bimodal metals have stimulated researchers to investigate their attractive mechanical performance experimentally and theoretically.

The pioneering work in bimodal materials was reported by Tellkamp et al.[7] and Wang et al.[4] respectively in relation to aluminium alloys and nanostructured copper, with regard to which high strength and high ductility, were both achieved. Since then, various experiments have been carried out to explore the mechanical performance of bimodal nanostructured metallic materials prepared through different technologies,[8–12] including a methodology involving cromilling and quasi-isostatic foging,[13] dynamic plastic deformation to induce static recrystallization[14,15] and a method combining the internal oxidation process and hot powder extrusion method.[16] These studies demonstrated that nano/ultrafine grains contribute to strengthening while good ductility is due to the coarse grains. With regard to bimodal materials, the existing dendrites,[8,17–19] cavitations on the surface of the deformed samples[10]

a)Email: llzhu@zju.edu.cn.

b)Corresponding author. Email: jianlu@cityu.edu.hk.

and microcracks arising in the matrix phase[9,20] are thought to be responsible for the fracture of these materials. The existing dendrites retard the propagation of the shear band and microcracks, and the cavitations and microcracks release the elastic stress at the interface between the large grains and nano/ultrafine grained phase. Theoretically, there have been some efforts to describe the constitutive behaviour and failure properties of bimodal metals/alloys.[21,22] Several continuum approaches have been adopted to simulate the stress-strain relationship in bimodal materials, including the Ramberg-Osgood formula combined with a finite-element method,[23] the secant Mori-Tanaka mean field approach[24] as well as the self-consistent scheme for elastic-viscoplastic materials.[25–27] Besides, a micromechanical model based on the analysis of localized deformation bands was presented to investigate the toughness behaviour of dual-phase composites including bimodal metals.[28] Unfortunately, there is no theoretical model that can capture completely the yield strength, strain hardening and ductility of bimodal metallic materials.

The maximum strength of nanotwinned copper was recently observed by experiment and the strain hardening and ductility were both significantly enhanced by decreasing the twin spacing.[29] In a similar way to grain boundaries (GBs) for strengthening materials, the twin boundaries (TBs) act as an effective barrier against dislocation motion and are potent strengtheners. The dislocations accumulated along the TBs facilitate a more uniform plastic deformation that in turn benefits the ductility of nanotwinned metals. However, there exists a fundamental difference in the plastic deformation affected by GBs and TBs. Atomistic simulations have confirmed that dislocation-TB interactions are the underlying mechanism for strengthening, strain hardening and toughening in nanotwinned metals.[30–34] For example, the pinning effects of TBs on dislocation contribute to the increase of yield strength,[35,36] and the gradual loss of coherence of TBs during deformation results in the high ductility of nanotwinned copper.[37] Furthermore, large-scale MD simulations were performed to give an insight into the softening mechanism in nanotwinned copper by further decreasing the twin spacing.[38] Besides these theoretical deformation mechanism studies, the continuum models were also presented to simulate the mechanical behaviour of nanotwinned polycrystalline metals. For example, two- and three-dimensional crystal plasticity models were developed by considering plastic anisotropy and rate-sensitive anisotropy to calculate the stress-strain relationship of nanotwinned metals.[39,40] Through incorporating the softening mechanism, a discrete twin crystal plasticity model was established with a focus on modelling the strengthening-softening yield transition in nanotwinned copper.[41] More recently, a unified mechanistic model was developed to characterize the size dependence of flow stress, activation volume and strain-rate sensitivity of nanocrystalline metals and nanotwinned metals.[42] The grain-size dependent critical twin spacing for the maximum yield strength in nanotwinned metals was also discussed by the MD simulation[38] and the continuum model.[43] Even though the twin-spacing dependent yield strength in nanotwinned metals has been captured by these continuum models, a quantitative description for strain hardening and tensile elongation still remains absent.

Recently, the authors and coworkers performed surface mechanical attrition treatment (SMAT) to prepare nanostructured metals with bimodal grain size distribution and nanotwinned polycrystalline metals in 304 stainless steels under various strain rates.[44] A good combination of high yield strength and high ductility was achieved in the proposed process. The dislocation-based plastic models were also developed to model the mechanical behaviour of bimodal nanostructured metals and nanotwinned metals.[45,46] The proposed model for the bimodal metal accounts for the impacts of the nano/microcracks in the nano/ultrafine grained phase during plastic deformation. The contribution of partial dislocations is taken into account in the model of nanotwinned metals as well as the competition of plastic deformation between the grain boundaries and twin lemallae. These models enable one to successfully describe the plastic deformation of these nanostructured metals. In the following, Section II briefly introduces a recent experimental study of nanostructured stainless steels with high strength and high ductility prepared by SMAT technology. Section III summarizes the recently developed theoretical models for bimodal metals and nanotwinned metals. Section IV presents the conclusion.

II. EXPERIMENT

Surface mechanical attrition treatment (SMAT) is an alternative top-down approach to produce nanostructured surface through the high-strain-rate deformation acting on the surface layer of a material. The nanostructuring mechanism and technology details involved in this approach have been extensively explored.[47,48] Here, an experimental study is introduced to shed some light on the relationship between the microstructures and mechanical properties of 304 stainless steel treated by SMAT over a wide range of strain rates.

A. SMATed sample with low strain rate

For austenitic stainless steel deformed under low strain rate ranging from $10\,s^{-1}$ to $10^3\,s^{-1}$, the deformation mechanism varies from dislocation gliding to martensite transformation, leading to ultrafine/nanograins formed near the surface of the samples. Nanograins arising on the surface are α'-matensite with random crystallographic orientations as shown in Fig. 1(a), and the grain size is in the range of 2–100 nm with a mean grain size of 10 nm as shown in Fig. 1(b).

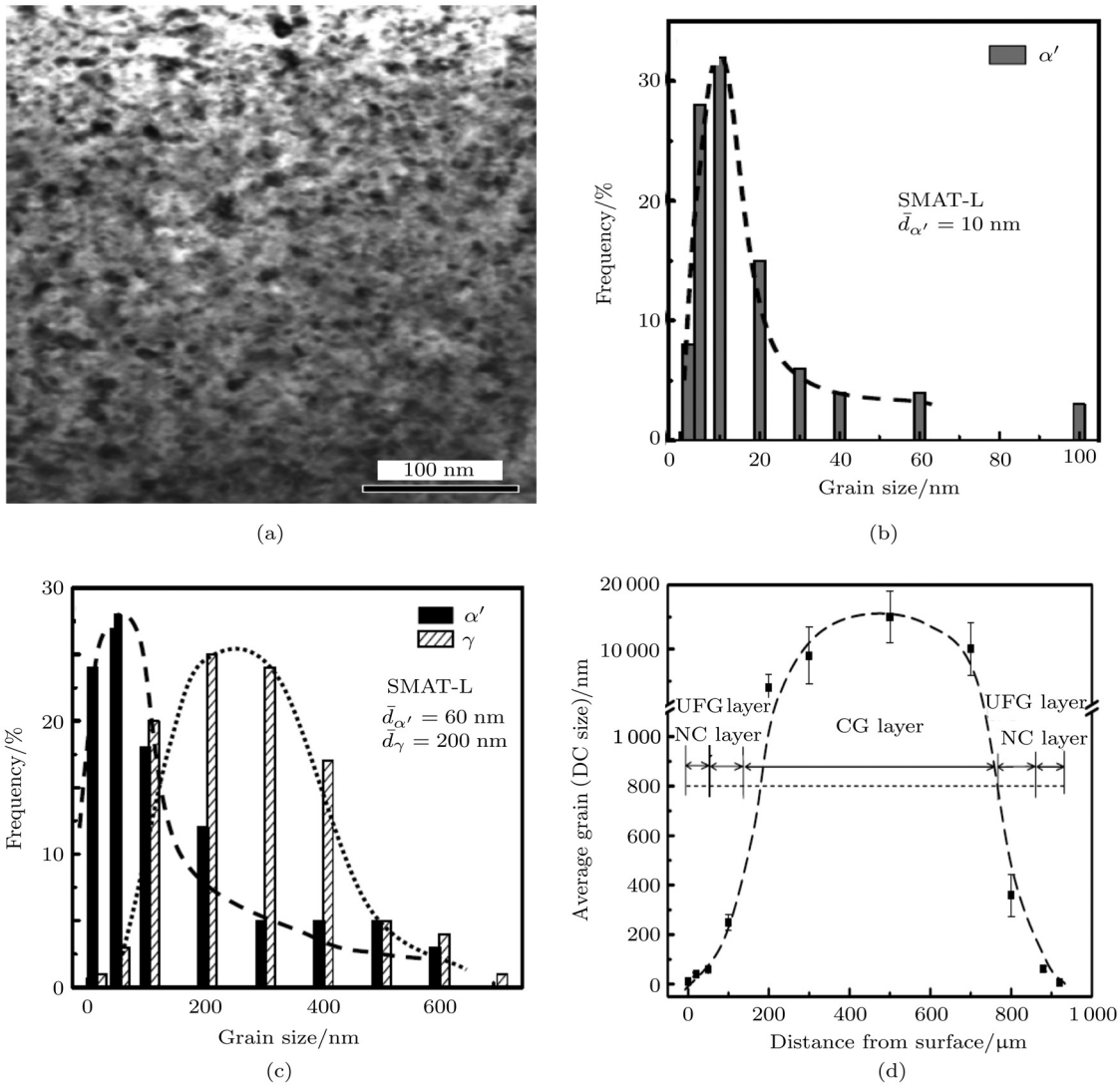

Fig. 1. Nanostructures of SMAT-L stainless steel with the bright-field TEM image (a), statistical distribution of grain size on the surface (b), statistical distribution of grain size of α'-martensite and γ-austenite phase (c), and the grain size/DC distribution (d).[44]

At a depth of 50 μm from the surface, the α'-martensite nanograins and the γ-austenite ultrafine grains are observed. These nanograins and ultrafine grains are uniformly distributed, as a result of the bimodal grain size distribution formed in these areas (see Fig. 1(c)). With increasing depth of the sample, the grain size grows from several nanometres to hundreds of nanometres within 150 μm (Fig. 1(d)). The microstructures of the SMAT sample with low strain rate can be regarded as a multimodel grain size distribution with a dual-phase structure.

B. SMATed sample with high strain rate

Under high strain rate in the range of 10^4 s^{-1} to 10^5 s^{-1}, martensite transformation is restrained and deformation twinning becomes the dominant deformation mechanism in the 304 stainless steels. As a consequence, there are numerous austenite nanotwins formed in the γ-austenite coarse grains as shown in Fig. 2(a). Meanwhile, a small fraction of α'-matensite and ε-matensite are also observed in the samples (Figs. 2(b) and 2(c)). At a depth of 300 μm, a typical twin-twin intersection can be observed as shown in Fig. 2(d), with the angle between the primary and the conjugate twins around 70.5°. The important feature on the microstructures in these samples is the high density of twins in the entire thickness with twin spacing from a few nanometres in the subsurface to a depth of hundreds of nanometres. Figure 2(e) shows that the twin spacing and twin density varied with depth from the surface. The twin spacing changes from 20 nm to 350 nm corresponding to a depth from 50 μm to the centre, and the twin density

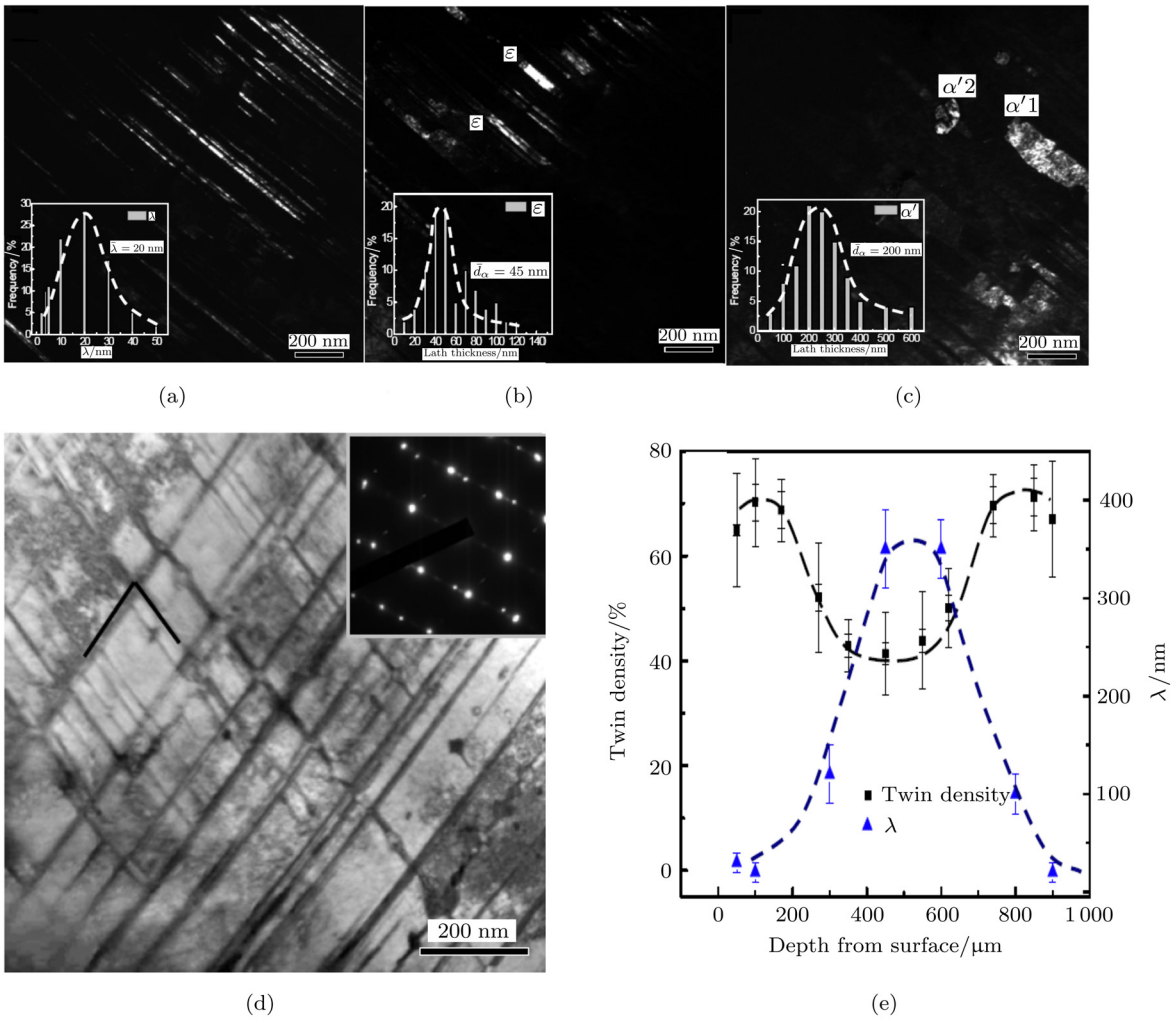

Fig. 2. Nanostructures in SMAT-H stainless steel with nanoscale twins (a), ε-martensite platelets (b), α'-martensite morphology (c), bright-field TEM image of intersection of twins (d), and twin density and twin thickness distribution (e).[44]

is from 65% to 40%.

C. Mechanical properties

The depth-dependent hardness is measured in the SMAT samples with low strain rate and high strain rate, as shown in Fig. 3(a). It is noted interestingly that the maximum hardness of the SMAT-L samples at 502 MPa is comparable with that of the SMAT-H samples at 495 MPa. The former is mainly contributed by the strengthening of nanograins and the latter by the nanotwins in the surface range. Due to a great number of deformation twins existing in the middle layer, the hardness of the SMAT-H sample at the centre is greater than that of the SMAT-L sample. Figure 3(b) further shows the stress-strain curves of the as-received, SMAT-L and SMAT-H samples. A good combination of high yield stress and high ductility is achieved in the SMAT samples. In the SMAT-L samples, the microstructure of nanograins provides high strength while the bimodal grain size distribution provides significant strain hardening capacity. With regard to the nanotwinned SMAT-H samples, the deformation twins block the dislocation motion and then strengthen the material, and the coarse grains remain able to maintain the good ductility of the material.

III. THEORETICAL MODELS

A. Bimodal metals

Experiments have demonstrated that nano/microcracks can be generated in the nano/ultrafine grained phase during plastic deformation and the density of these cracks increases with further deformation. Inspired by these observations, the impacts of the nano/microcracks on the plastic deformation of bimodal metals will be considered. Firstly, the

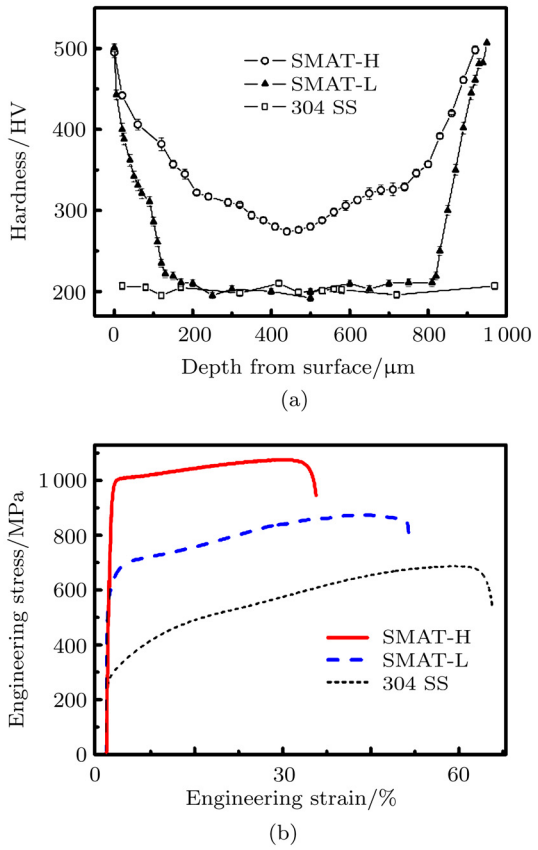

Fig. 3. Hardness distribution with depth (a) and engineering stress-strain curves (b) of the SMAT samples and as-received stainless steel.[44]

nano/microcracks release the elastic stress around the cracks to alter the stress-strain statics in the nano/ultrafine grained phase. Secondly, the increase of these cracks drive more dislocations stopped along the grain boundaries, giving rise to the back stress effect in the nano/ultrafine grained phase. Here, the micromechanical composite model[49] is adopted to simulate the global stress-strain response, and the strain gradient plastic theory is applied in each constituent phase. In the following, we summarize the formulae of the model.

Since bimodal metals are considered to be composed of the nano/ultrafine grained phase and the coarse grained phase (see Fig. 4(a)), the modified mean field approach is utilized to determine the overall stress and stress in bimodal materials. The relationship between the hydrostatic and deviatoric strains and stresses of the constituent phases and those of the composite follows

$$
\begin{aligned}
&\varepsilon_{kk}^{(0)} = (A_0 + A_2)\bar{\varepsilon}_{kk}, \quad \varepsilon'^{(0)}_{ij} = B_2\bar{\varepsilon}'_{ij} - c_1 B_1 \varepsilon^{\mathrm{p}(1)}_{ij},\\
&\varepsilon_{kk}^{(1)} = A_0\bar{\varepsilon}_{kk}, \quad \varepsilon'^{(1)}_{ij} = B_0\bar{\varepsilon}'_{ij} + c_0 B_1 \varepsilon^{\mathrm{p}(1)}_{ij},\\
&\sigma_{kk}^{(0)} = 3\kappa_0(A_0 + A_2)\bar{\varepsilon}_{kk},\\
&\sigma'^{(0)}_{ij} = 2\mu_0^{\mathrm{s}}[(B_0 + B_2)\bar{\varepsilon}'_{ij} - c_1 B_2 \varepsilon^{\mathrm{p}(1)}_{ij}],\\
&\sigma_{kk}^{(1)} = 3\kappa_0 A_1\bar{\varepsilon}_{kk},\\
&\sigma'^{(1)}_{ij} = \frac{2\mu_0^{\mathrm{s}}}{\beta_0^{\mathrm{s}}} B_2[\bar{\varepsilon}'_{ij} - (1 - c_0\beta_0^{\mathrm{s}})\varepsilon^{\mathrm{p}(1)}_{ij}],
\end{aligned}
\tag{1}
$$

where

$$
\begin{aligned}
A_0 &= \frac{\kappa_0}{c_0\alpha_0^{\mathrm{s}}(\kappa_1 - \kappa_0) + \kappa_0},\\
A_1 &= \frac{\kappa_1}{c_0\alpha_0^{\mathrm{s}}(\kappa_1 - \kappa_0) + \kappa_0},\\
A_2 &= \frac{\alpha_0^{\mathrm{s}}(\kappa_1 - \kappa_0)}{c_0\alpha_0^{\mathrm{s}}(\kappa_1 - \kappa_0) + \kappa_0},\\
B_0 &= \frac{\mu_0^{\mathrm{s}}}{c_0\beta_0^{\mathrm{s}}(\mu_1 - \mu_0^{\mathrm{s}}) + \mu_0^{\mathrm{s}}},\\
B_1 &= \frac{\beta_0^{\mathrm{s}}\mu_1}{c_0\beta_0^{\mathrm{s}}(\mu_1 - \mu_0^{\mathrm{s}}) + \mu_0^{\mathrm{s}}},\\
B_2 &= \frac{\beta_0^{\mathrm{s}}(\mu_1 - \mu_0^{\mathrm{s}})}{c_0\beta_0^{\mathrm{s}}(\mu_1 - \mu_0^{\mathrm{s}}) + \mu_0^{\mathrm{s}}}.
\end{aligned}
\tag{2}
$$

Here, c_i is the volume fraction of the ith phase, and κ_i and μ_i are the bulk and shear moduli of the ith phase, respectively. α_0^{s} and β_0^{s} are the components of Eshelby's tensor for spherical inclusions following $S_0^{\mathrm{s}} = (\alpha_0^{\mathrm{s}}, \beta_0^{\mathrm{s}})$, in which $\alpha_0^{\mathrm{s}} = (1 + \nu_0^{\mathrm{s}})/3(1 - \nu_0^{\mathrm{s}})$ and $\beta_0^{\mathrm{s}} = 2(4 - 5\nu_0^{\mathrm{s}})/15(1 - \nu_0^{\mathrm{s}})$. The secant bulk and shear moduli of the ith phase are taken to satisfy the isotropic relations as $k_i^{\mathrm{S}} = E_i^{\mathrm{S}}/[3(1 - 2\nu_i^{\mathrm{S}})], \mu_i^{\mathrm{S}} = E_i^{\mathrm{S}}/[2(1 + \nu_i^{\mathrm{S}})]$, where the secant Young's modulus is written as $E_i^{\mathrm{S}} = E_i/[1 + (E_i\varepsilon^{(i)}/\sigma_{\mathrm{flow}}^{(i)})(\sigma_{11}^{(i)}/\sigma_{\mathrm{flow}}^{(i)})^{m_0 - 1}]$ and secant Poisson's ratio is $\nu_i^{\mathrm{S}} = 1/2 - (1/2 - \nu_i E_i^{\mathrm{S}}/E_i)$ for the ith phase. Therefore, the dilatational and deviatoric stresses and strains of the composite are connected by

$$
\begin{aligned}
&\bar{\sigma}_{kk} = 3\kappa_0\left[1 + c_1(A_1 - A_0)\right]\bar{\varepsilon}_{kk},\\
&\bar{\sigma}'_{ij} = 2\mu_0^{\mathrm{s}}\left[\left(1 + \frac{c_1 B_2}{\beta_0^{\mathrm{s}}}\right)\bar{\varepsilon}'_{ij} - \frac{c_1 B_1}{\beta_0^{\mathrm{s}}}\varepsilon^{\mathrm{p}(1)}_{ij}\right].
\end{aligned}
\tag{3}
$$

It should be pointed out that the flow stress in the coarse grained phase is different from the one in the nano/ultrafine grained phase. The flow stress in the coarse grain phase is expressed as

$$
\sigma_{\mathrm{flow}}^{1} = \sigma_0 + M\alpha\mu b\sqrt{\rho_{\mathrm{I}}} + \sigma_{\mathrm{b}}. \tag{4}
$$

Here, α, μ and M are the empirical constant, the shear modulus and the Taylor factor, respectively. σ_0 is the lattice friction stress, σ_{b} is the back stress and ρ_{I} is the density of dislocations in the crystal interiors which can be obtained from Kocks and Mecking's model.[50] The flow stress of the nano/ultrafine grained phase can be expressed by

$$
\sigma_{\mathrm{flow}}^{0} = \sigma_0 + M\alpha\mu b\sqrt{\rho_{\mathrm{I}} + \rho_{\mathrm{GB}}}, \tag{5}
$$

where $\rho_{\mathrm{GB}} = k^{\mathrm{GB}}\eta^{\mathrm{GB}}/b$ is the density of dislocations and $k^{\mathrm{GB}} = 6d_{\mathrm{GBDPZ}}/\phi^{\mathrm{GB}}d_{\mathrm{G}}$.

For the sake of accounting for the impact of nano/microcracks on plastic deformation, the nano/microcrack-matrix-effective-medium approach[51] is utilized to model the overall stress and strain in the nano/ultrafine grained phase of bimodal metals. Thus, the corresponding effective moduli follow

$$
E_1 = E_0\left[1 + \frac{16(1 - \nu_0^2)\rho}{3}\right]^{-1},
$$

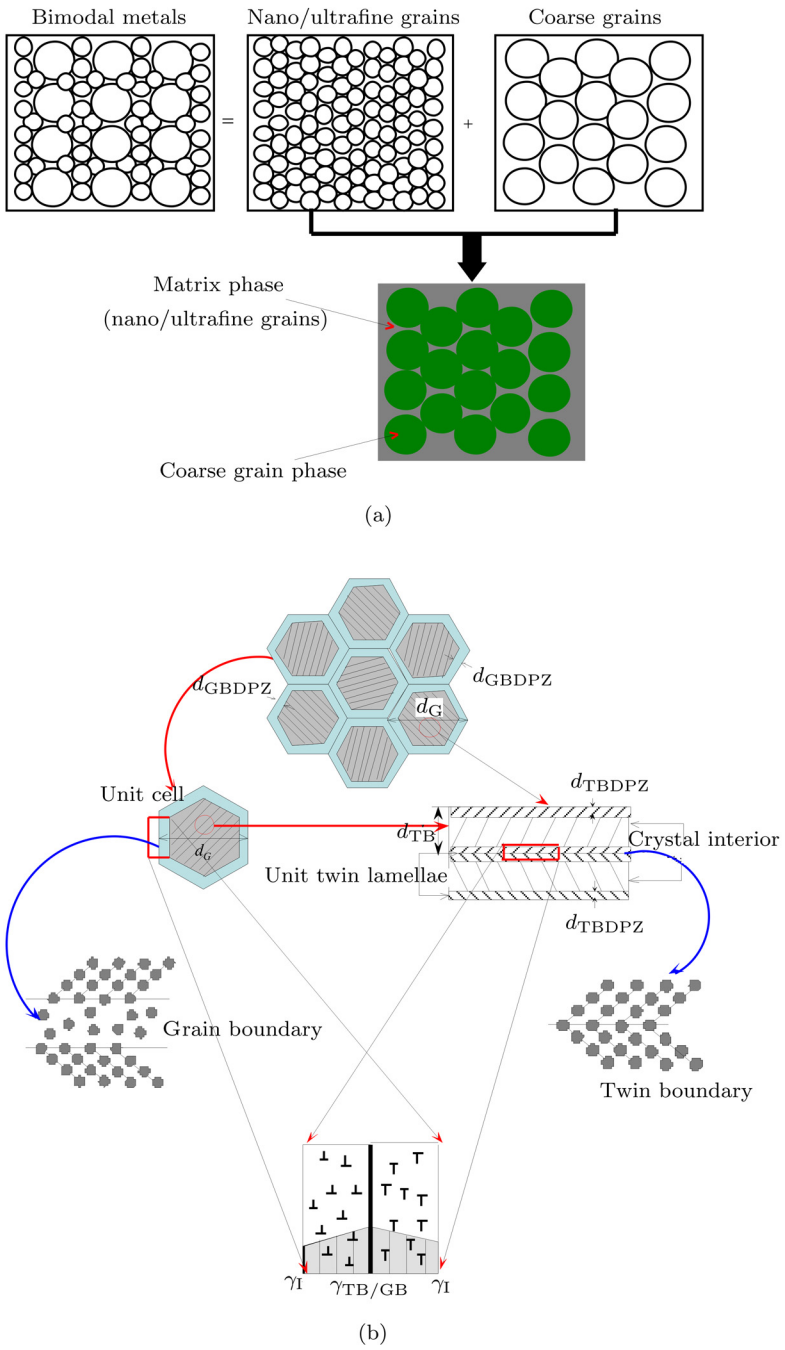

Fig. 4. Schematic drawings of the proposed model for bimodal metals (a) and nanotwinned polycrystalline metals (b).[45,46]

$$G_{12} = G_0 \left[1 + \frac{8(1+\nu_0)\rho}{3(1-\nu_0/2)}\right]^{-1}, \tag{6}$$

where $\rho = \rho_0 P(f_W) = \rho_0(1 - f_W(\varepsilon_p))$is the density of nano/microcracks, ρ_0 represents the maximum density of nano/microcracks in the nano/ultrafine grained phase, $f_W(\varepsilon_p) = \exp[-(\varepsilon_p/\varepsilon_0)^m]$ is the strain-based Weibull distribution function, ε_0 is the reference strain and m is the Weibull modulus. The arising back stress in the nano/ultrafine grained phase can be expressed by

$$\sigma_b^* = M\frac{\mu b}{d_G}N^*. \tag{7}$$

Here, N^* is the number of dislocations stopped at the grain boundaries, following the evolution law of $N^* = N_0^*\{1 - \exp[-\zeta^*\varepsilon^p/(bN_0^*)]\}$ where ζ^* is the mean spacing between slip bands that results from the generation of nano/microcracks, and N_0^* is the maximum number of dislocation loops at the grain boundaries in the nano/ultrafine grained phase.

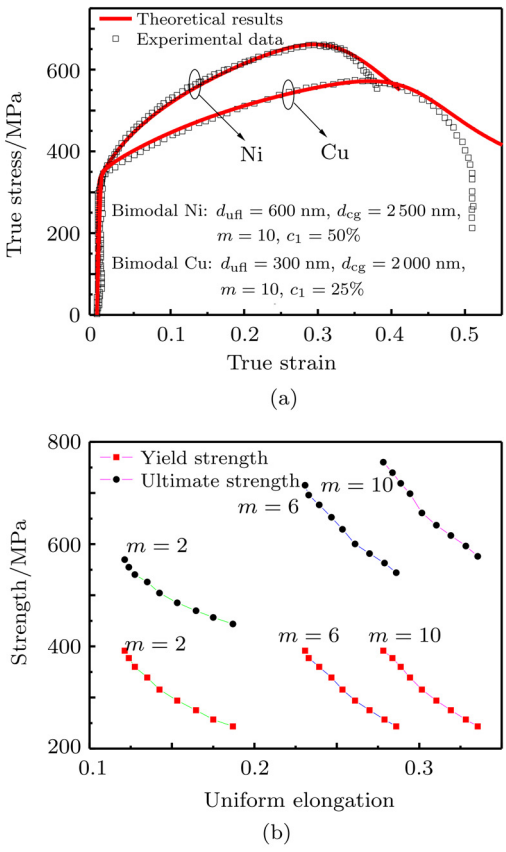

Fig. 5. Comparison of the stress-strain relationship between the theoretical results and the experiments for bimodal metals (a), and relationship between strength and uniform elongation with different Weibull moduli for bimodal nickel (b).[45]

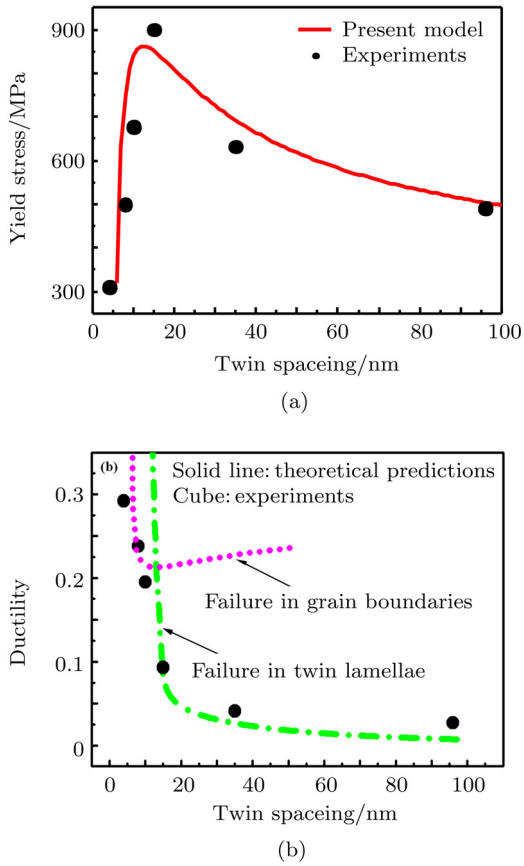

Fig. 6. Predicted yield stress (a) and ductility (b) of nanotwinned copper as functions of twin spacing in comparison with experimental data.[46]

B. Nanotwinned metals

During plastic deformation in nanotwinned polycrystalline metals, a great number of dislocations accumulate along the grain boundaries and twin boundaries. Therefore, the dislocation pileup zones nearby the GBs (GBDPZ) and the TBs (TBDPZ) are introduced in the proposed model as shown in Fig. 4(b). In these regions, the strain gradients are involved to define the dislocation density of the GBDPZ and TBDPZ. By decreasing the twin spacing in the nanotwinned metal, the number of partial dislocations is increased in turn, leading to the deformation mechanism changing from dislocation-TB interactions to twinning partial dislocations. Consequently, the contributions of partial dislocations are taken into account in our analysis in the strain hardening and strain gradient in the TBDPZ. We summarize the formulae of the proposed model for bimodal metals in the following.

Due to the existence of the strain gradient in the GB/TBDPZ, strain gradient plasticity is utilized here to describe the stress-strain response in the materials. According to the Taylor model, the flow stress in the nanotwinned metals can be expressed by

$$\sigma_{\text{flow}} = \sigma_0 + M\alpha\mu b\sqrt{\rho} + \sigma_{\text{b}}, \tag{8}$$

where α, μ and M are the Taylor constant, shear modulus and Taylor factor, respectively; σ_0 is the lattice friction stress and σ_{b} denotes the back stress that induces kinematic hardening; $\rho = \rho_{\text{I}} + \rho_{\text{TB}} + \rho_{\text{GB}}$ is the total density of dislocations; ρ_{TB}, ρ_{GB} and ρ_{I} denote the dislocation densities in the TBDPZ, GBDPZ and crystal interior, respectively. The dislocation density in the TBDPZ is written as $\rho_{\text{TB}} = k^{\text{TB}}\tilde{\eta}^{\text{TB}}/b$, where $k^{\text{TB}} = 12d_{\text{TBDPZ}}/\phi^{\text{TB}}\pi d_{\text{TB}}$, and the local strain gradient in the TBDPZ $\tilde{\eta}^{\text{TB}}$ is expressed as

$$\tilde{\eta}^{\text{TB}} = \eta_1 d_{\text{TB}} + \eta_0 - \eta_P/d_{\text{TB}}. \tag{9}$$

Here, $\eta_1 = \phi^{\text{TB}}N_0 b/(d_{\text{TBDPZ}}d_G^2)$ and $\eta_0 = \phi^{\text{TB}}n_p' b/[(d_{\text{TBDPZ}}d_G\sqrt{3})\eta_P] = \sqrt{3}\pi\phi_p b/(12d_{\text{TBDPZ}})$, n_p' being the number of initial twinning partials in the TBDPZ, N_0 the maximum number of inclined dislocations in a grain, d_{TB} the twin spacing, d_{TBDPZ} the thickness of TBDPZ, and ϕ_p and ϕ^{TB} are geometric factors.

To evaluate the ductility of nanotwinned metals, a new failure criterion is proposed as follows

$$\tau_{\text{flow}} \geq \tau_{\text{crit}}. \tag{10}$$

It is assumed that the unit twin lamella or grain boundaries start to fail as soon as the local flow stress exceeds the critical stress for spontaneous nucleation of dislocations in these regions. The local shear flow stress in the unit twin lamella and the GBDPZ can be presented as

$$\tau_{\text{flow}}^{\text{TB}} = \alpha\mu b\sqrt{\rho_{\text{I}}^{\text{unit}} + \rho_{\text{TB}}^{\text{unit}}} + \tau_{\text{b}},$$
$$\tau_{\text{flow}}^{\text{GB}} = \alpha\mu b\sqrt{\rho_{\text{GB}}} + \tau_{\text{b}}. \quad (11)$$

The critical stress to nucleate a new dislocation has been determined in the framework of a continuum model described by Asaro and Rice.[52]

C. Numerical results and comparisons

After identifying the parameters of the models through extraction from the literature or comparison with the experiments, the numerical results of bimodal metals based on the proposed model are shown in Fig. 5(a) as well as the experimental data. Clearly noted from the figure is that the proposed model can successfully describe the yield strength, strain hardening and ductility, and good agreement is obtained in comparison with the measurements. The further predictions for yield strength and ductility as the functions of the volume fraction of coarse grains are plotted in Fig. 5(b). By decreasing the volume fraction of coarse grain, the strength of bimodal metal is reinforced while the ductility becomes weaker. Based on the developed model for the nanotwinned metals, the predicted yield strength and ductility of nanotwinned copper are shown in Fig. 6 as the functions of twin spacing. The experimental data are also plotted in the figures. The predictions are in good accordance with the experimental data, including the critical twin spacing for maximum yield strength of 13 nm consistent with the measurement of 15 nm. Another interesting finding is that the failure occurs in the twin lamellae for the large twin spacing while the grain boundaries prefer to fail when the twin spacing is very small. Furthermore, the proposed model of nanotwinned metals indicates that the critical twin spacing is dependent on the grain size linearly, which agrees with the results from MD simulations.[38]

IV. CONCLUSION

Generating internal boundaries in polycrystalline metals and mixing various microstructures of different size in nanostructured materials have been substantiated as alternative methodologies to achieve high yield strength and high ductility. Surface mechanical attrition treatment (SMAT) as an efficient technology for nanostructuring the surface of a material, can be used to prepare nanostructured metal with bimodal/multimodal grain size distribution and the nanotwinned polycrystalline metals. The mechanism-based plastic models developed recently for nanotwinned metals and bimodal metals enable the provision of theoretical approaches for designing the microstructures in nanostructured metals, leading to optimizing the mechanical performance of such materials. Inspired by these studies, various new nanostructured metals can be engineered theoretically and experimentally in the future by involving nanotwins, bi/multi-modal grain size distribution and phase transformation, in which a good combination of high strength and good ductility can be achieved.

The authors are thankful to Elsevier for their permission to reuse the Figures. This work was supported by the Chinese Ministry of Science and Technology of China (2012CB932203), the Research Grants Council of the Hong Kong Special Administrative Region of China (CityU8/CRF/08 and GRF/CityU519110), the Croucher Foundation CityU9500006 and PolyU Postdoctoral Fellowship Project (G-YX3S).

1. K. Lu, L. Lu, and S. Suresh, Science **324**, 349 (2009).
2. L. Lu, Y. F. Shen, and X. H. Chen, et al, Science **304**, 422 (2004).
3. M. Dao, L. Lu, and R. J. Asaro, et al, Acta Mater. **55**, 4041 (2007).
4. Y. M. Wang, M. W. Chen, and F. H. Zhou, et al, Nature **419**, 912 (2002).
5. X. Zhang, A. Misra, and H. Wang, et al, Acta Mater. **52**, 995 (2004).
6. Y. F. Shen, L. Lu, and M. Dao, et al, Scripta Mater. **55**, 319 (2006).
7. V. L. Tellkamp, A. Melmed, and E. J. Lavernia, Metall. Mater. Trans. **A2**, 2335 (2001).
8. G. He, J. Eckert, and W. Löser, et al, Nature Mat. **2**, 33 (2003).
9. B. Q. Han, Z. Lee, and D. Witkin, et al, Metall. Mater. Trans. A **36**, 957 (2005).
10. G. J. Fan, H. Choo, and P. K. Liaw, et al, Acta Mater. **54**, 1759 (2006).
11. S. H. Xia, L. V. Vychigzhanina, and J. T. Wang, et al, Mater. Sci. Eng. A **490**, 471 (2008).
12. M. J. N. V. Prasad, S. Suwas, and A. H. Chokshi, Mater. Sci. Eng. A **503**, 86 (2009).
13. Y. H. Zhao, T. Topping, and J. F. Bingert, et al, Adv. Mater. **20**, 3028 (2008).
14. Y. S. Li, Y. Zhang, and N. R. Tao, et al, Scripta Mater. **59**, 475 (2008).
15. S. Shekhar, J. Cai, and J. Wang, et al, Mater. Sci. Eng. A **527**, 187 (2009).
16. H. Simchi, and A. Simchi, Mater. Sci. Eng. A **507**, 200 (2009).
17. G. He, M. Hagiwara, and J. Eckert, et al, Phil. Mag. Lett. **84**, 365 (2004).
18. J. Das, A. Güth, and H. J. Klauβ, et al, Scripta Mater. **49**, 1189 (2003).
19. J. Das, W. Löser, and U. Kühn, et al, Appl. Phys. Lett. **82**, 4690 (2003).
20. Z. H. Lee, V. Radmilovic, and B. Ahn, et al, Metall. Mater. Trans. A **41**, 795 (2010).
21. V. A. Pozdnyakov, Tech. Phys. Letts. **33**, 1004 (2007).
22. G. A. Malygin, Phys. Solid State **50**, 1032 (2008).
23. R. Q. Ye, B. Q. Han, and E. J. Lavernia, Metall. Mater. Trans. A **36**, 1833 (2005).

24. S. P. Joshi, K. T. Ramesh, and B. Q. Han, et al, Metall. Mater. Trans. A **37**, 2397 (2006).
25. S. Berbenni, V. Favier, and M. Berveiller, Int. J. Plasticity **23**, 114 (2007).
26. B. Raeisinia, C. W. Sinclair, and W. J. Poole, et al, Modelling Simul. Mater. Sci. Eng. **16**, 025001 (2008).
27. S. Ramtani, G. Dirras, and H. Q. Bui, Mech. Mater. **42**, 522 (2010).
28. S. H. Xia, and J. T. Wang, Int. J. Plasticity **26**, 1442 (2010).
29. L. Lu, X. Chen, and X. Huang, et al, Science **323**, 607 (2009).
30. Z. H. Jin, P. Gumbsch, and E. Ma, et al, Scripta Mater. **54**, 1163 (2006).
31. Z. H. Jin, P. Gumbsch, and K. Albe, et al, Acta Mater. **56**, 1126 (2008).
32. A. J. Cao, Y. G. Wei, and S. X. Mao, Appl. Phys. Lett. **90**, 151909 (2007).
33. A. Froseth, H. Van Swygenhoven, and P. M. Derlet, Acta Mater. **52**, 4041 (2004).
34. A. Froseth, P. M. Derlet, and H. Van Swygenhoven, Appl. Phys. Lett. **85**, 5863 (2004).
35. K. A. Afanasyev, and F. Sansoz, Nano Lett. **7**, 2056 (2007).
36. Y. G. Zheng, J. Lu, and H. W. Zhang, et al, Scripta Mater. **60**, 508 (2009).
37. T. Zhu, J. Li, and A. Samanta, et al, Proc. Natl. Acad. Sci. **104**, 3031 (2007).
38. X. Y. Li, Y. J. Wei, and L. Lu, et al, Nature **464**, 877 (2010).
39. M. Dao, L. Lu, and Y. Shen, et al, Acta Mater. **54**, 5421 (2006).
40. A. Jerusalem, M. Dao, and S. Suresh, et al, Acta Mater. **56**, 4647 (2008).
41. H. Mirkhani, and S. P. Joshi, Acta Mater. **59**, 5603 (2011).
42. P. Gu, M. Dao, and R. J. Asaro, et al, Acta Mater. **59**, 6961 (2011).
43. Y. J. Wei, Phys. Rev. B **83**, 132104 (2011).
44. A. Y. Chen, H. H. Ruan, and J. Wang, et al, Acta Mater. **59**, 3697 (2011).
45. L. L. Zhu, H. H. Ruan, and X. Y. Li, et al, Acta Mater. **59**, 5544 (2011).
46. L. L. Zhu, and J. Lu, Int. J. Plasticity **30-31**, 166 (2011).
47. H. W. Zhang, Z. K. Hei, and G. Liu, et al, Acta Mater. **51**, 1871 (2003).
48. H. L. Chan, H. H. Ruan, and A. Y. Chen, et al, Acta Mater. **58**, 5086 (2010).
49. G. J. Weng, J. Mech. Phys. Solid **38**, 419 (1990).
50. U. F. Kocks, and H. Mecking, Prog. Mater. Sci. **48**, 171 (2003).
51. M. Kachanov, Adv. Appl. Mech. **30**, 259 (1994).
52. R. J. Asaro, and J. R. Rice, J. Mech. Phys. Solids **25**, 309 (1977).